Heterogeneity and growing length scales in the dynamics of kinetically constrained lattice gases in two dimensions

Albert C. Pan,[1] Juan P. Garrahan,[2] and David Chandler[1]
[1]*Department of Chemistry, University of California, Berkeley, California 94720-1460, USA*
[2]*School of Physics and Astronomy, University of Nottingham, Nottingham, NG7 2RD, United Kingdom*
(Received 27 June 2005; published 28 October 2005)

We study dynamical heterogeneity and growing dynamical length scales in two kinetically constrained models, namely, the one- and two-vacancy assisted triangular lattice gases. One of the models is a strong glassformer and the other is a fragile glassformer. Both exhibit heterogeneous dynamics with broadly distributed time scales as seen in the distribution of persistence times. We show that the Stokes-Einstein relation is violated, to a greater degree in the fragile glassformer, and show how this violation is related to dynamic heterogeneity. We extract dynamical length scales from structure factors of mobile particles and show, quantitatively, the growth of this length scale as density increases. We comment on how the scaling of lengths and times in these models relates to that in facilitated spin models of glasses.

DOI: 10.1103/PhysRevE.72.041106 PACS number(s): 05.20.Jj, 05.70.Jk, 64.70.Pf

I. INTRODUCTION

The dramatic dynamical slowdown accompanying the formation of a glass is a remarkable phenomenon [1–3]. One explanation for the underlying microscopic cause of this slowdown relies on the presence of local steric constraints on the movement of particles, which make themselves felt to an increasing degree as the temperature is lowered (or the concentration of particles is increased). Kinetically constrained lattice gas models [4–6] are simple caricatures of glassformers which employ local steric constraints as their sole means to glassiness in the *absence* of any nontrivial static correlations between particles (for alternative thermodynamic views of the glass transition, see, e.g. [7,8]). These constrained models have been extensively studied (see, e.g. [4,5,9–11]). Our purpose here is to extend these studies to focus on the idea of dynamical heterogeneity [12–14] as a manifestation of excitation lines in space time and to attempt identification of scaling and universality classes in the dynamics of these models [15–19].

The paper is organized as follows. Section II describes the two models we use as well as details of the computer simulations used to study them. Section III looks at heterogeneous dynamics in our models via the distribution of persistence times. Section IV presents the scaling of the structural relaxation time and diffusion constant, the implications of which lead to a discussion of the breakdown of the Stokes-Einstein relation in Sec. V. Section VI discusses the emergence of a dynamical length scale and gives a quantitative characterization of this length by analyzing structure factors of mobile particles. Finally, we end with a discussion of our results in Sec. VII.

II. MODELS AND COMPUTATIONAL DETAILS

We present results for two kinetically constrained triangular lattice gas (TLG) models introduced by Jäckle and Krönig [5]. These two-dimensional models are variants of lattice models proposed by Kob and Andersen [4]. Each site of the triangular lattice has six nearest neighbor sites and can hold at most one particle. A particle at site $\mathbf{i}$ is allowed to move to a nearest neighbor site, $\mathbf{i}'$, if (i) $\mathbf{i}'$ is not occupied and (ii) the two mutual nearest neighbor sites of $\mathbf{i}$ and $\mathbf{i}'$ are also empty. These rules coincide with a physical interpretation of steric constraints on the movement of hard core particles in a dense fluid [5]. We call the model with these rules the (2)-TLG because both mutual nearest neighbors need to be empty in order to facilitate movement. We also present results for the (1)-TLG where the constraints are more relaxed: movement is allowed as long as either of the mutual nearest neighbors is empty. As with other kinetically constrained lattice gas models, the TLG has no static interactions between particles other than those that prohibit multiple occupancy of a single lattice site. Therefore initial configurations can be generated by random occupation of empty lattice sites by particles until the desired density is reached.

In the computer simulations, we investigated particle densities, ρ, between 0.01 and 0.80 for the (2)-TLG and between 0.01 and 0.996 for the (1)-TLG. The density $\rho=1$ corresponds to the completely full lattice in both cases. For the (2)-TLG, we used a lattice with edge length $L=128$ for all densities. There exists the possibility in the (2)-TLG of initial configurations containing an unmoveable structure which percolates throughout the system called a backbone [4,5]. Since the dynamics obey detailed balance, these backbones could never be destroyed in the course of the simulation. For the densities studied here, however, $L=128$ is sufficiently large such that the probability of having such a configuration is vanishingly small (see [5]). For the (1)-TLG, we used $L=128$ to 2048. A pair of vacancies in the (1)-TLG can always diffuse freely [5] so this version of the TLG does not suffer from the problem of backbones in the same way as the (2)-TLG. At higher densities, however, one still needs to ensure that there are a sufficient number of potentially mobile particles in the system such that the typical dynamics of the model are observed. For the (1)-TLG, the number of potentially mobile particles at higher densities is approximately equivalent to the number of vacancy pairs and therefore can

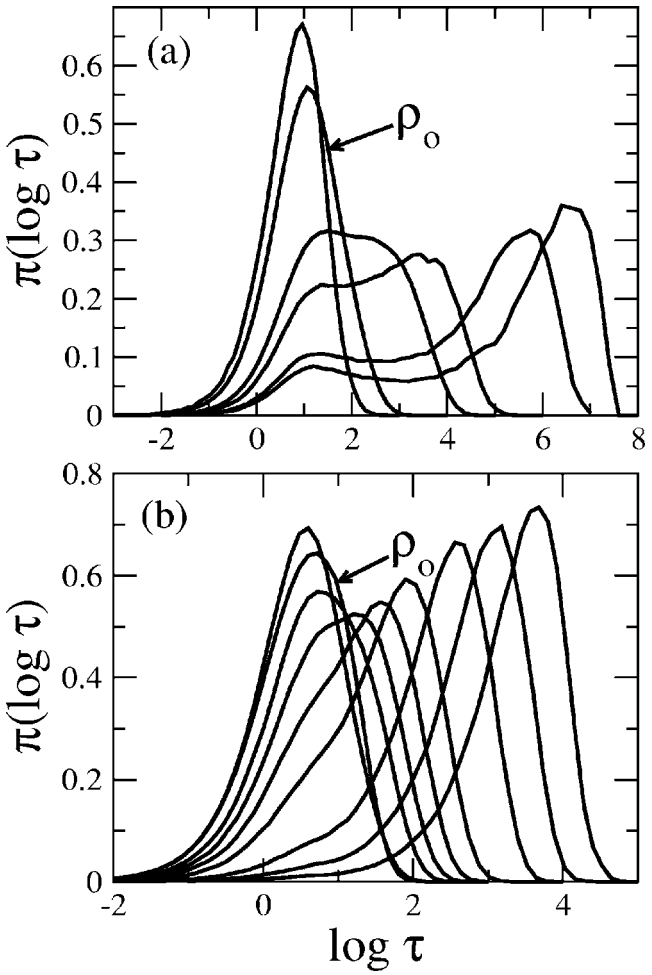

FIG. 1. Distribution of local persistence times for (a) the (2)-TLG model (from left to right) $\rho=0.40$, 0.50, 0.65, 0.70, 0.77, and 0.79; and (b) the (1)-TLG model (from left to right) $\rho=0.20$, 0.60, 0.70, 0.75, 0.80, 0.85, 0.92, 0.95, and 0.97. The density is defined as the number of particles divided by the total system size, L^2, such that a density of one indicates a completely full lattice. The abscissae are given on a scale of logarithm base 10. The unit of time is Monte Carlo sweeps. The density, ρ_o, is the onset density discussed in the text.

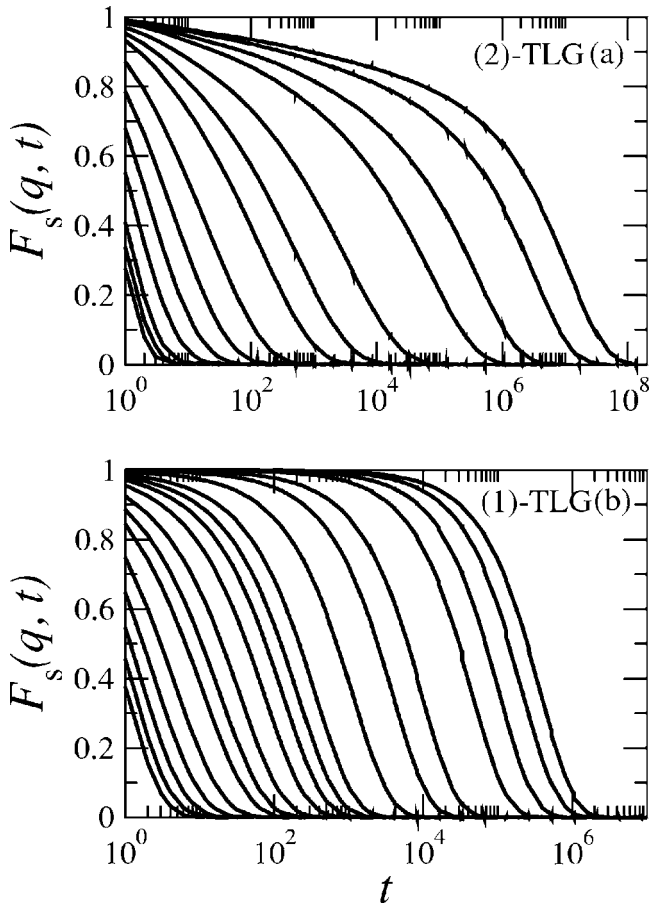

FIG. 2. Self-intermediate scattering function at wave vector $\mathbf{q}=(\pi,0)$ for (a) the (2)-TLG (from left to right) $\rho=0.01$, 0.05, 0.10, 0.20, 0.30, 0.40, 0.50, 0.60, 0.65, 0.70, 0.75, 0.77, 0.79, and 0.80; and (b) the (1)-TLG (from left to right) $\rho=0.20$, 0.30, 0.40, 0.50, 0.60, 0.70, 0.75, 0.80, 0.85, 0.88, 0.90, 0.92, 0.95, 0.97, 0.98, 0.99, 0.993, 0.995, and 0.996. The unit of length is the lattice spacing.

be estimated as $(1-\rho)^2L^2$. The system sizes at the various densities for the (1)-TLG simulations were chosen such that the number of potentially mobile particles estimated in this way was always approximately 100. For both models, periodic boundary conditions were used.

At each density, several hundred independent trajectories of lengths 10–100 times τ_α, where τ_α is the time for the self-intermediate scattering function at $\mathbf{q}=(\pi,0)$ [21] to reach $1/e$ of its initial value (see below), were run. Trajectories were stored logarithmically for later analysis (i.e., configurations were saved after 1, 2, 4, 8, 16, 32, etc. sweeps). At each state point, between 128 and 256 independent trajectories were acquired. Time was measured in Monte Carlo sweeps. During each sweep, particles were chosen randomly and a move was attempted. For the higher density runs in both models, a continuous time algorithm was used for greater efficiency [22]. This algorithm involved making and updating a list of only those particles which have the possibility of moving and choosing from among those exclusively during every move. The total time (in units of Monte Carlo sweeps) was then updated accordingly by adding to it the inverse of the number of mobile particles available during that continuous time step. The continuous time algorithm resulted in a speed up of our simulations by as much as one to two orders of magnitude for the highest density runs in both the (1)-TLG and the (2)-TLG. Finally, for the distribution of site persistence times (see below), statistics were gathered over runs of very large systems ($L=1024$ and 2048).

III. HETEROGENEOUS DYNAMICS AND THE DISTRIBUTION OF PERSISTENCE TIMES

A central phenomenon behind our perspective of glasses is dynamical heterogeneity [12,13]. A direct measure of heterogeneous dynamics in glassy systems is the idea of persistence times [16,17]. Figures 1(a) and 1(b) show the distribution of site persistence times, $\pi(\log \tau)$, in the (2)-TLG and (1)-TLG at various densities; that is, the distribution of

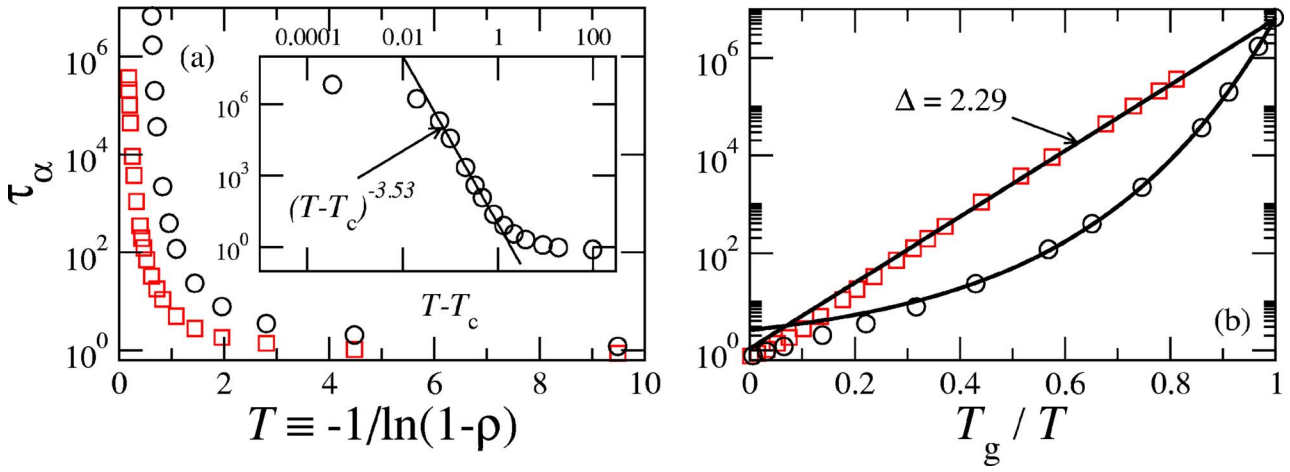

FIG. 3. (Color online) (a) Structural relaxation time as a function of temperature. Circles and squares correspond to the (2)-TLG and (1)-TLG, respectively, throughout the paper. The inset shows the same data for the (2)-TLG plotted vs $T-T_c$ and a power law fit (solid line) to a portion of the data. (b) Structural relaxation as a function of scaled reciprocal temperature. Here T_g is such that $\tau_\alpha(T_g)=10^7$. The lines are fits to the relaxation times at low temperatures. For the (1)-TLG we use the Arrhenius form $\ln \tau_\alpha \propto \Delta/T$, with $\Delta \approx 2.29$. For the (2)-TLG we use a double exponential [10], $\ln \tau_\alpha \propto \exp(a/T)$, with $a \approx 1.76$.

times, given an initial configuration of the lattice, before the first change at a particular site occurs, either due to an empty site being filled or a filled site becoming empty. These distributions are multipoint functions because they depend not only on the state of a lattice site at the initial time and the time when it changes, but also on all intervening points in time. As has been shown in spin-facilitated models [16], three distinct dynamical regimes are observed: (i) at low densities, there is a single peak at small relaxation times indicating homogeneous fast dynamics; (ii) at intermediate densities, two peaks develop and coexist, one at faster times and the other at slower times, indicating heterogeneous, fluctuation dominated, dynamics; and (iii) as density is increased even higher, the peak at faster times becomes suppressed relative to the peak at slower times and the dynamics again become homogeneous and slow. In region (ii), or the crossover region, the dynamics are broadly distributed over several orders of magnitude in time. Following [16], we can define, qualitatively, an onset density, ρ_o, for both models where the dynamics begin to feel the influence of dynamical heterogeneity and thereby lose their mean-field character, as well as a crossover density ρ_c where slow processes begin to dominate. For the (2)-TLG, $\rho_o=0.50$ and (we anticipate) $\rho_c=0.80$ and for the (1)-TLG, $\rho_o=0.60$ and $\rho_c=0.85$.

In the next section, we turn to two two-point functions which have been the more conventional measures of glassy dynamics: the self-intermediate scattering function and the mean-squared displacement.

IV. DYNAMICAL SLOWDOWN

A basic ingredient of a glassformer is a precipitous dynamical slowdown over a narrow range of temperatures or densities. This characteristic can already be seen qualitatively in the distribution of persistence times by looking at the movement of the mean of the distributions as ρ increases. For example, in the (2)-TLG, from $\rho=0.70$ to 77, the mean persistence time increase two to three orders of magnitude. The traditional measure of this slowdown is the self-intermediate scattering function, $F_s(q,t)=\langle e^{i\mathbf{q}\cdot[\mathbf{r}_i(t)-\mathbf{r}_i(0)]}\rangle$, particularly its decay at wave vector $\mathbf{q}=(\pi,0)$, Figs. 2(a) and 2(b). Here, $\mathbf{r}_i(t)$ denotes the position of particle i at time t. The angled brackets, $\langle\cdots\rangle$, denote an average over different pairs of configurations along a trajectory separated by a given time interval. The decay of the scattering function to $1/e$ at this wave vector is typically defined to be τ_α, or the structural relaxation time, as it gives a sense of how density fluctuations relax at relatively short length scales.

Experiments report the scaling of viscosity versus inverse temperature, $1/T$. Therefore, for the particular case of a kinetic lattice gas, one would like to make connections between structural relaxation time and viscosity, and density and inverse temperature. In both experiments and computer simulations [23,24], it has been shown that the structural relaxation time scales like the viscosity. We imagine that the logarithm of the vacancy concentration, $1-\rho$, is proportional to the logarithm of the concentration of excitations, c, where $\ln c$ is, to within an additive constant, proportional to inverse temperature as in spin-facilitated Ising models [6]. That is, to within additive and multiplicative constants, $\ln(1-\rho) \sim \ln c \sim -1/T$. It is reasonable, therefore, to define an effective temperature as

$$-\ln(1-\rho) \equiv 1/T. \tag{1}$$

In other words, there is an analogy between the triangular lattice gas models and excitation models which is made explicit by this particular definition of temperature as we discuss below.

The structural relaxation time plotted versus T and $1/T$ is shown in Figs. 3(a) and 3(b), respectively. The inset of Fig. 3(a) shows a plot of τ_α versus $T-T_c$ for the (2)-TLG where T_c is taken to be the temperature at the crossover density, ρ_c (as defined in Sec. III), and the black line is a power law fit to a portion of the data in the manner of mode coupling

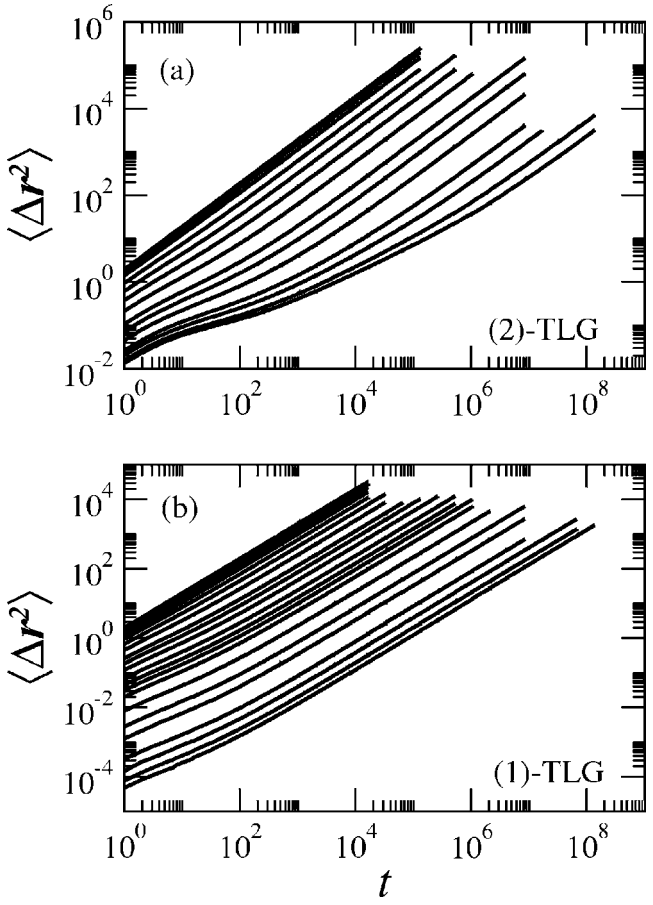

FIG. 4. The mean-squared displacement: (a) the (2)-TLG, ρ =0.01 to 0.80; and (b) the (1)-TLG, ρ=0.01 to 0.996.

theory (MCT) [25]. In MCT, T_c is a critical temperature where time scales diverge. We see that the MCT fit is valid for almost five orders of magnitude in time even though there is no dynamical arrest at T_c, as the relaxation time of the (2)-TLG diverges only at ρ=1 [5,10]. A similar MCT

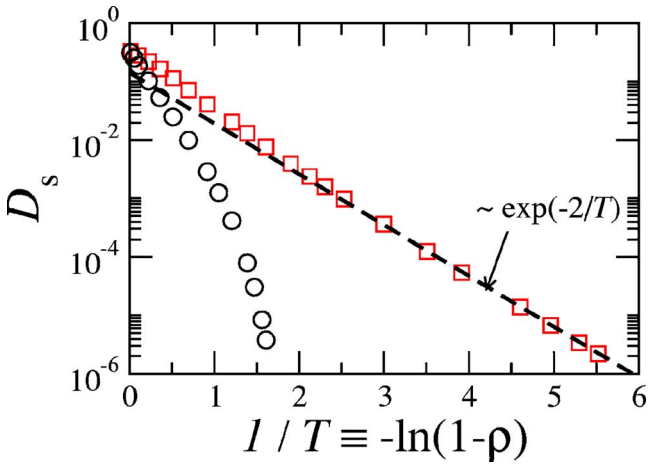

FIG. 5. (Color online) Self-diffusion constant as a function of inverse effective temperature. At low temperatures, the self-diffusion constant for the (2)-TLG fits well to $\exp[-2.5\exp(1/T)]$ and that of the (1)-TLG fits well to $\exp(-2/T)$.

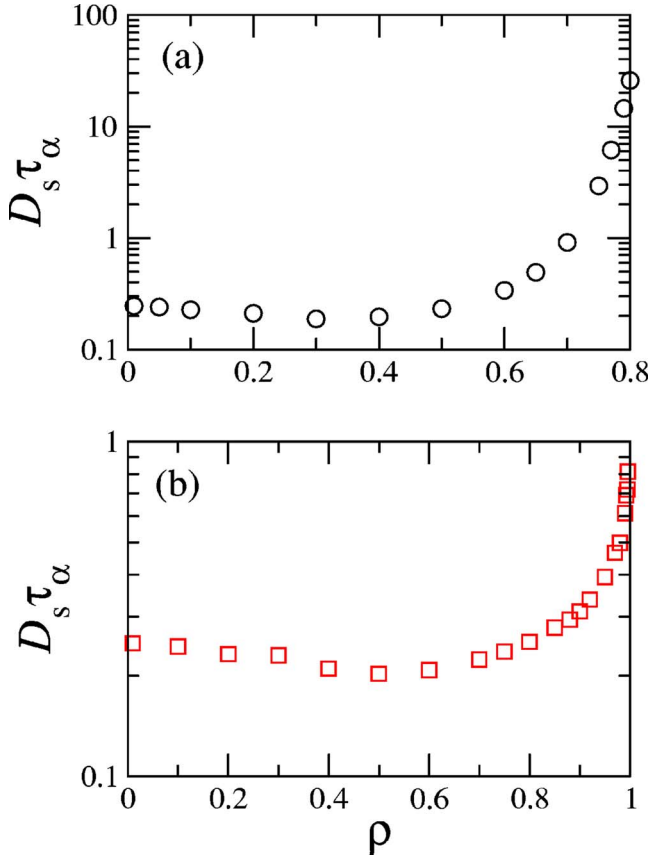

FIG. 6. (Color online) Stokes-Einstein violation in the (a) (2)-TLG and (b) (1)-TLG.

power law fit (not shown) can be made for the (1)-TLG, valid for about two orders of magnitude.

Figure 3(b) shows the relaxation time on a reduced temperature scale in the manner proposed by Angell [2]. Here, T_g is defined as the temperature at which $\tau_\alpha = 10^7$. We see that the relaxation time of the (1)-TLG is Arrhenius growing as $\tau_\alpha \sim c^{-\Delta}$ with $\Delta = 2.29$, as $\rho \to 1$. The relaxation of the (2)-TLG in contrast is super-Arrhenius, and the low temperature data can be fit with a double exponential in $1/T$ [10]. That is, $\ln \tau_\alpha \sim \text{const} + \ln c$ for the (1)-TLG and $\ln \tau_\alpha \sim \text{const} + f(c)\ln c$, where $f(c)$ is some function of the concentration of excitations, for the (2)-TLG. These temperature behaviors follow from the fact that the dynamics of the excitations in the (1)-TLG is diffusive while the dynamics of the excitations in the (2)-TLG is hierarchical. In this context, the (1)-TLG is a strong glassformer whereas the (2)-TLG is a fragile one. It is often the case in experiment that strong glassformers are networked materials. We have argued elsewhere, however, that any material will obey strong scaling at large enough relaxation times and this behavior arises from the diffusive dynamics of the underlying mobility field [15,20].

Interestingly, the time exponent $\Delta \approx 2.3$ of the (1)-TLG is the same as that for the one-spin facilitated Fredrickson-Andersen (FA) model in dimension $d=2$, obtained in renormalization group (RG) calculations and observed numerically [18]. This suggests that the (1)-TLG may be in the universality class of the FA model, the prototypical kineti-

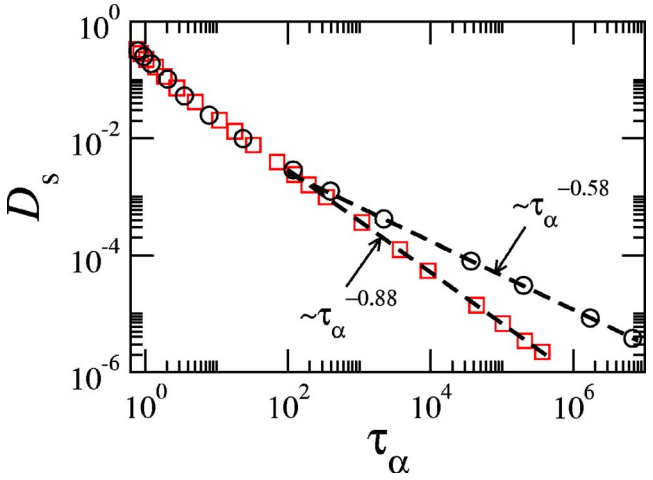

FIG. 7. (Color online) Fractional Stokes-Einstein exponent: scaling of the self-diffusion constant with relaxation time. The dashed lines are fits to the data at longer times.

cally constrained spin model for a strong glassformer [26]. We will examine more of these dynamic scaling relations below.

The mean-squared displacement, $\langle|\Delta\mathbf{r}_i(t)|^2\rangle=\langle|\mathbf{r}_i(t)-\mathbf{r}_i(0)|^2\rangle$, is shown in Fig. 4. The self-diffusion coefficient, D_s, is defined as $D_s=\lim_{t\to\infty}\langle|\Delta\mathbf{r}_i(t)|^2\rangle/4t$. We see that at low densities, D_s for the (1)-TLG and (2)-TLG coincide. At higher densities, D_s for the (1)-TLG is Arrhenius, and scales as $D_s\sim c^2$ as $\rho\to 1$, see Fig. 5. This result is in agreement with the analytical predictions of [5,10]. Moreover, this is also the scaling of the diffusion constant for a probe molecule coupled to the FA model in any dimension [17], further evidence that the (1)-TLG is in the FA model universality class. On the other hand, D_s for the (2)-TLG is super-Arrhenius (see Fig. 5). The behavior of D_s is similar, qualitatively, to that of τ_α. The quantitative difference in their scaling with density, however, is significant, and is an indication that relaxation behaviors at short and long length scales are not the same. We turn to this issue now in both the (1)-TLG and the (2)-TLG.

V. THE BREAKDOWN OF THE STOKES-EINSTEIN RELATION

An important ramification of broadly distributed heterogeneous dynamics is the breakdown of mean-field dynamical relations such as the much studied Stokes-Einstein (SE) relation. This relation says that diffusion scales inversely with the relaxation time, $D_s\tau_\alpha\sim$ constant. It is a quantitative statement of the expectation that the dynamical behavior of normal liquids should be similar at all but the smallest length scales. In supercooled liquids this simple mean-field approximation fails [28,29], and, given the results of previous sections, we would expect a similar violation of the SE relation

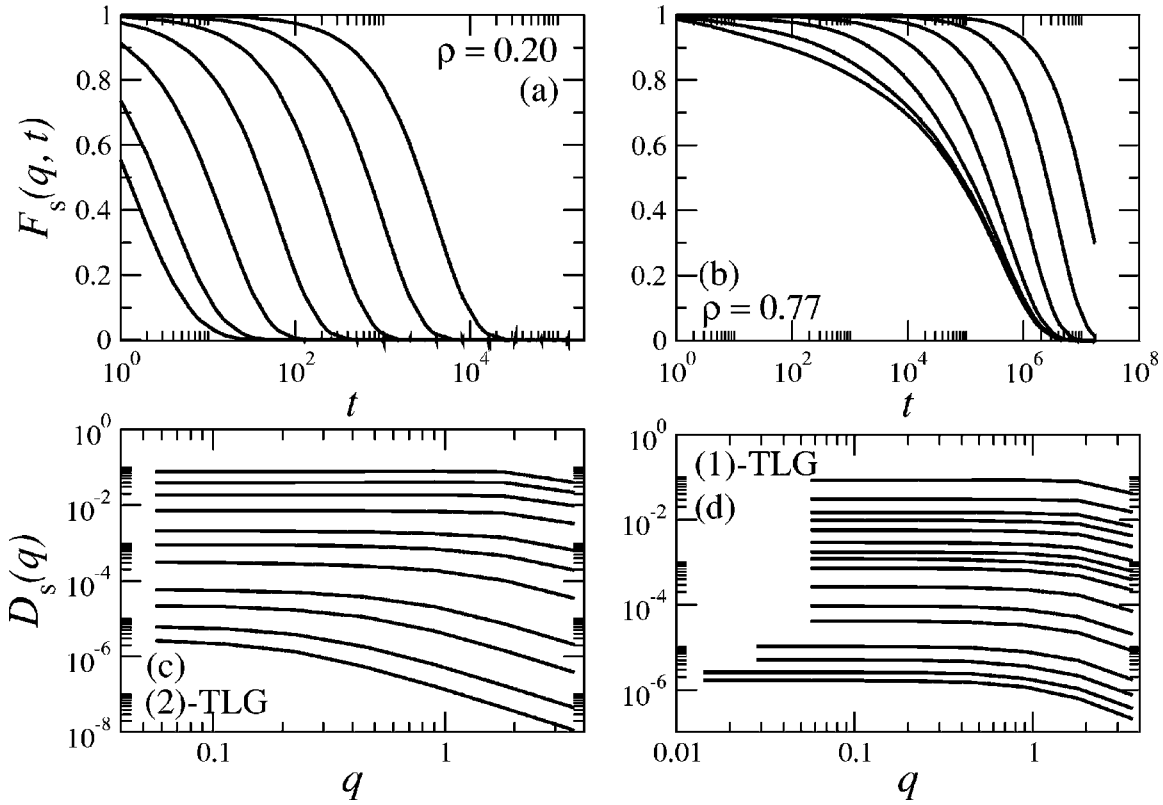

FIG. 8. (Top) Self-intermediate scattering function for the (2)-TLG at various wave vectors: (a) $\rho=0.20$ and (b) $\rho=0.77$. For both graphs, from left to right: $q=(\pi,0)$, $(\pi/2,0)$, $(\pi/4,0)$, $(\pi/8,0)$, $(\pi/16,0)$, $(\pi/32,0)$, and $(\pi/64,0)$. (Bottom) $D_s(q)\equiv 1/\tau(q)q^2$ as a function of q at various densities: (c) (2)-TLG, (from top to bottom) $\rho=0.20$ to 0.80 and (d) (1)-TLG (from top to bottom), $\rho=0.40$ to 0.996. The higher density curves for the (1)-TLG include smaller q values because of larger system sizes (see Sec. II).

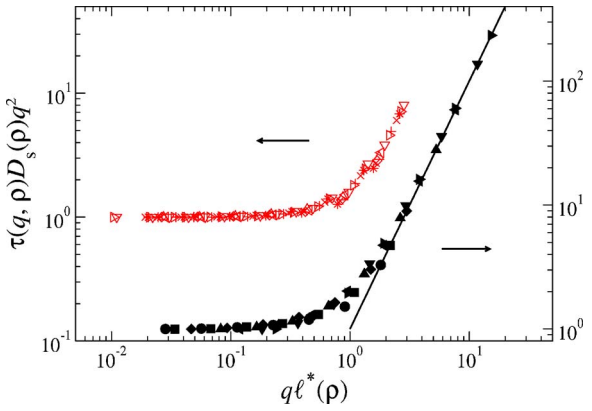

FIG. 9. (Color online) Data from Fig. 8 collapsed onto a master curve. The closed symbols correspond to the (2)-TLG and the open symbols correspond to the (1)-TLG. The straight line is q^2.

in the TLG models. We see from Fig. 6 that the SE relation is indeed violated for both the (2)-TLG and the (1)-TLG, the effect being more pronounced in the fragile case. Moreover, we see that the densities at which the product $D_s\tau_\alpha$ begins deviating from constancy coincide with the onset densities, ρ_o's, extracted from the distribution of persistence times. This observation reinforces the idea that it is the fluctuation dominated nature of the dynamics that leads to the SE breakdown [17].

SE violation implies that the self-diffusion constant does not scale with the structural relaxation time as τ_α^{-1}. One possibility is that it obeys a fractional SE law, $D_s \sim \tau_\alpha^{-\xi}$ where $\xi < 1$. This is observed in experiments [28], and is obtained theoretically for probe diffusion in the FA and East models [17] (see also [30]). Figure 7 shows that the diffusion constant also obeys a fractional SE law in the TLG models. The SE exponent is $\xi \approx 0.88$ for the (1)-TLG, which is the value expected for the FA model in $d=2$, $\xi \approx 2/2.3$ [17]. In the case of the (2)-TLG, despite the fact that D_s and τ_α are both

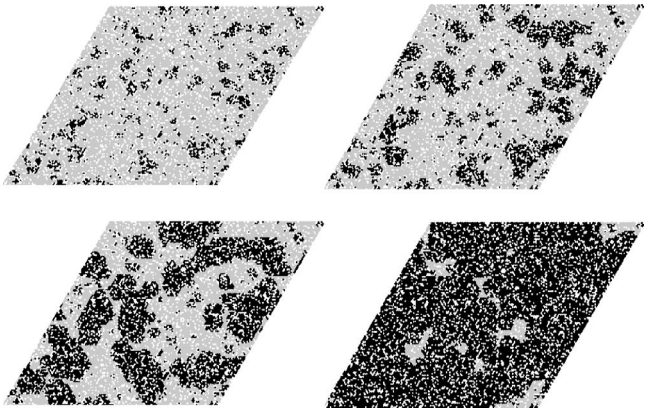

FIG. 10. Growth of mobile particle regions as a function of observation time Δt at $\rho=0.77$ in the (2)-TLG. Black and gray regions indicate the location of particles and white regions indicate empty lattice sites. Particles colored in black have moved at least one lattice spacing in a time Δt whereas particles colored in gray have not. (Top, from left to right: $\Delta t = 10^3$ and 10^4; bottom, from left to right: $\Delta t = 10^5$ and 10^6; $\tau_\alpha \sim 10^5$ at this density).

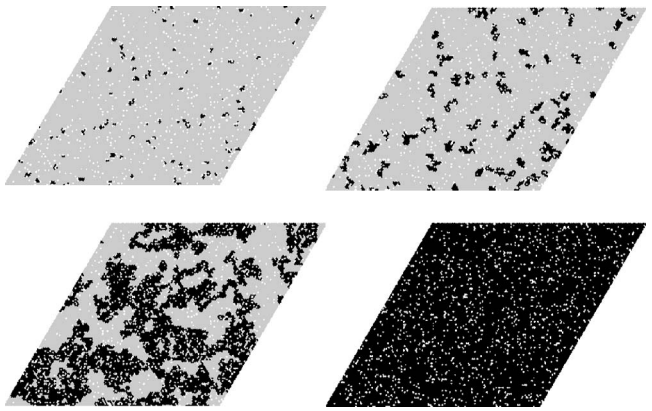

FIG. 11. Same as Fig. 10 for the (1)-TLG. Here, $\rho=0.95$. (Top, from left to right: $\Delta t = 10$ and 10^2; bottom, from left to right: $\Delta t = 10^3$ and 10^4; $\tau_\alpha \sim 10^3$ at this density.)

super-Arrhenius, we find that the scaling exponent is temperature independent at large densities, $\xi \approx 0.58$. The deviation of this exponent from 1 is larger than that for both the FA and East models in two dimensions [17]. It indicates a larger violation of the SE law, consistent with the fact that the (2)-TLG is more fragile than either of those models [10].

VI. DYNAMICAL LENGTH SCALES

A. Indication of a dynamical length scale from a two-point function

Since the growth in time scales and the violation of the Stokes-Einstein relation in the TLG models are clearly not tied to a growth in static length scales, we turn now to the discussion of dynamical length scales. Such a length scale can be inferred from examining the relaxation behavior of the self-intermediate scattering function over more than one wave vector at different densities. One can appreciate this fact qualitatively by looking at the decay of $F_s(q,t)$ for the (2)-TLG over several values of q at low and high density, Fig. 8 (top) [19]. At low density, the decay of the various curves looks similar at all wave vectors (except for the largest wave vector) whereas at high density, even the curves at intermediate wave vector differ greatly from the simple exponential form seen at smaller wave vectors. The high density curves bunch up at intermediate to large $\mathbf{q}$ indicating that the relaxation behavior at these length scales is different (i.e., slower) than one would expect from the behavior at larger length scales [5]. Similar behavior has also been observed in the Kob-Andersen kinetic lattice gas model and kinetically constrained spin models [4,19].

To quantify the above behavior, we proceed as in [31,32]. In the hydrodynamic regime, we have $\lim_{q\to 0} F_s(q,t) \sim \exp(-D_s q^2 t)$, and one expects the product $D_s\tau(q)q^2$ to be independent of $\mathbf{q}$, where $\tau(q)$ is the time when the intermediate scattering function at wave vector $\mathbf{q}$ decays to $1/e$. In Fig. 8 (bottom), we plot the quantity $D_s(q) \equiv 1/\tau(q)q^2$ as a function of q at various densities. A flat line independent of q indicates normal diffusive behavior whereas a downward bend signifies a change to subdiffusive behavior. As density

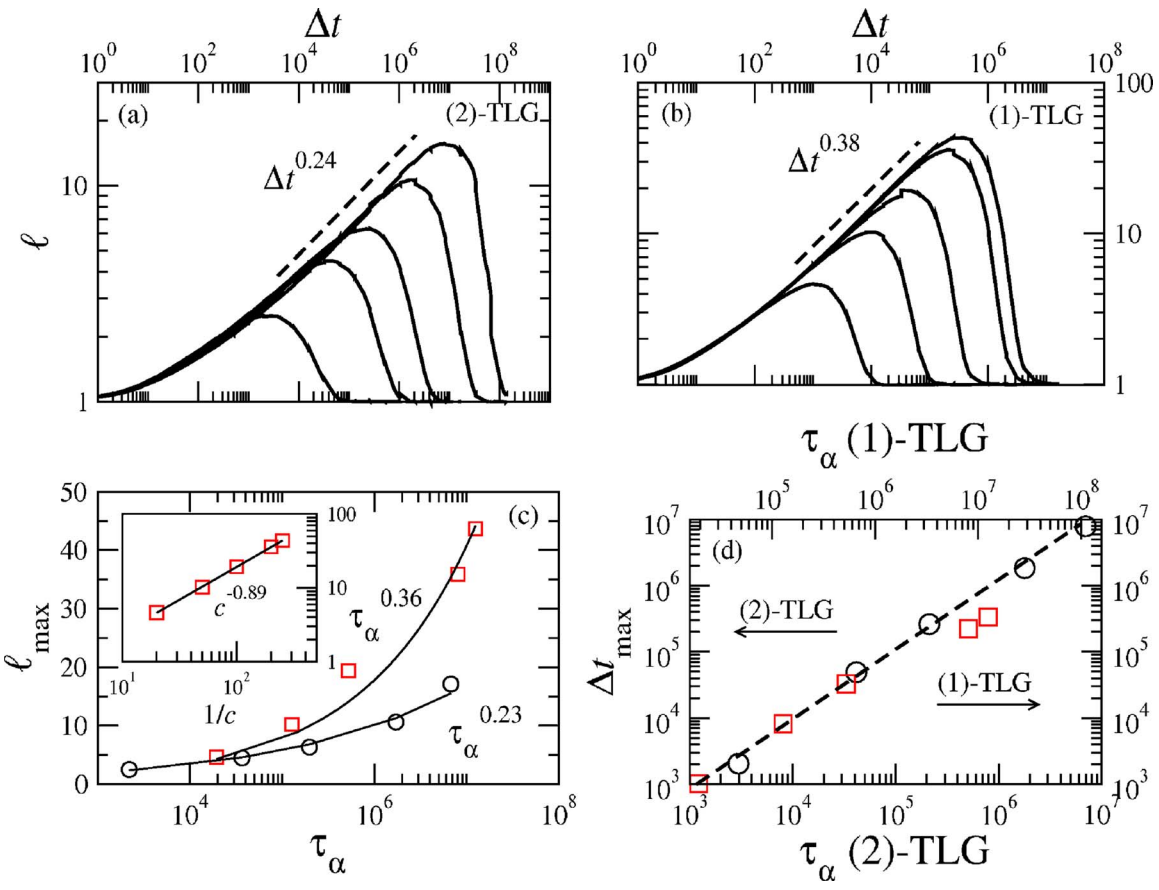

FIG. 12. (Color online) (Top) Growth of dynamical heterogeneity length as a function of observation time, Δt, for (a) the (2)-TLG, $\rho = 0.70$ to 0.80; and (b) the (1)-TLG, $\rho = 0.95$ to 0.996. (Bottom) (c) Scaling of the maximum value of the dynamical heterogeneity length, ℓ_{max}, from (a) and (b) with relaxation time. The inset shows ℓ_{max} vs c for the (1)-TLG, on a log-log scale to highlight power law scaling. (d) The scaling of the structural relaxation time, τ_α, with Δt_{max}, the value of the observation time at ℓ_{max}. The dashed line is τ_α^{-1}.

increases, the curves begin to bend at a smaller and smaller wave vector, q^*. This behavior is indicative of a growing dynamical length scale as density is increased [19,31,32].

Following the prescription of [19], we extract a length scale, ℓ^*, from Fig. 8 as $\ell^* \sim \sqrt{D_s(q \to 0)\tau_\alpha}$. This length scale determines the onset of Fickian diffusion. Using ℓ^* to rescale space, and using $\tau(q)q^2$ to rescale time, the data from Fig. 8 can be collapsed onto a master curve, Fig. 9.

B. Direct observation and quantification of a dynamical heterogeneity length scale

We can study dynamical length scales in the TLG models directly by observing a trajectory over a time Δt and coloring particles which have moved at least one lattice spacing. Snapshots of applying this procedure to trajectories of the (2)-TLG and the (1)-TLG at high particle densities over progressively longer Δt's are shown in Figs. 10 and 11. Mobility is indeed correlated: mobile particles are clustered and the clusters of mobility at earlier Δt act as seed particles from which subsequent mobility grows. Moreover, there is a qualitative difference in the shape of the clusters in the (2)-TLG and the (1)-TLG. In the fragile model, the clusters are smooth and more anisotropic, indicating a directed growth of mobile regions. In the strong model, the clusters are rugged and isotropic. These observations can be understood as arising from the difference in the local constraints of both models. The strict two site facilitation rule of the (2)-TLG requires cooperative, hierarchical rearrangement of particles for movement whereas the one site facilitation rule of the (1)-TLG allows for the random diffusion of vacancy pairs [5]. These same correlations between fragility and the smoothness of interfaces and between slow and fast dynamically heterogeneous regions are present in other facilitated models [15,18,33].

To quantify the above ideas, we extract a dynamical length scale, $\ell(\Delta t)$, from structure factors of the mobile particles [13,15,31,34]. Motivated by the mobility criterion described in the previous paragraph and depicted in Figs. 10 and 11, we consider the following binary field:

$$n_{\mathbf{r}}(t) = \sum_i \delta(\mathbf{r}_i(t) - \mathbf{r})(1 - \delta(\mathbf{r}_i(t + \Delta t) - \mathbf{r}_i(t))). \qquad (2)$$

Here, $\mathbf{r}_i(t)$ denotes the position of the ith particle at time t, $\delta(\mathbf{x})$ is the Kronecker delta function, and the sum is over all particles. This field, $n_{\mathbf{r}}(t)$, is one if the particle at $\mathbf{r}$ has moved at least one lattice spacing in time Δt and zero otherwise. Note that it will not count as mobile particles which, in time Δt, have moved away from, but returned to, their origi-

nal site. It will, however, count particles which have exchanged places or are moving in a string-like single file manner. Its structure factor is a four point function: it measures a correlation function which depends on two points in time, t and $t+\Delta t$, and two points in space, $\mathbf{r}$ and $\mathbf{r}'$.

We define the structure factor for the mobility field as the following normalized correlation function:

$$S(\mathbf{q};\Delta t) = \frac{1}{L^2}\frac{\langle \delta n_{\mathbf{q}}(t;\Delta t)\,\delta n_{-\mathbf{q}}(t;\Delta t)\rangle}{\langle \delta n_{\mathbf{r}}(t;\Delta t)^2\rangle}, \tag{3}$$

where $\delta n_{\mathbf{r}}(t;\Delta t) = n_{\mathbf{r}}(t;\Delta t) - \langle n_{\mathbf{r}}(t;\Delta t)\rangle$ is the deviation of $n_{\mathbf{r}}$ from its average value and $\delta n_{\mathbf{q}}(t;\Delta t)$ is the Fourier transform of $\delta n_{\mathbf{r}}(t;\Delta t)$:

$$\delta n_{\mathbf{q}}(t;\Delta t) = \sum_{\mathbf{r}} \exp\left(\frac{2\pi i}{L^2}\mathbf{r}\cdot\mathbf{q}\right)\delta n_{\mathbf{r}}(t;\Delta t). \tag{4}$$

The angled brackets, $\langle\cdots\rangle$, denote an average over different pairs of configurations along a trajectory separated by a given time interval Δt. We then define the length scale, $\ell(\Delta t)$, to be proportional to the inverse of the first moment, $\bar{q}_{\Delta t}$, of the circularly averaged structure factor, $\tilde{S}(q_n;\Delta t)$ [35]. That is, $\ell(\Delta t) \sim 1/\bar{q}_{\Delta t}$ where

$$\bar{q}_{\Delta t} = \sum_n q_n \tilde{S}(q_n;\Delta t)/\sum_n \tilde{S}(q_n;\Delta t). \tag{5}$$

Here, $q_n = 2\pi n/L$ and $n = 0,1,2,\ldots,L/2$. The length scale was normalized such that ℓ extracted from the structure factor of a random configuration of particles on the lattice (i.e., an ideal gas) was unity. The length scale $\ell(\Delta t)$ is the typical linear size of correlated dynamical domains at observation time Δt in units of lattice spacings.

Figures 12(a) and 12(b) show $\ell(\Delta t)$ at various densities for the (2)-TLG and the (1)-TLG. The basic shape of these curves is as expected: as $\Delta t \to 0$, mobility is sparse and uncorrelated so ℓ approaches unity and as $\Delta t \to \infty$, everything becomes mobile and ℓ once again tends towards unity. In between, as the pictures in Figs. 10 and 11 suggest, mobility clusters together and grows. Looking at the maximum of these different curves, $\ell_{\max}(\Delta t_{\max})$, a growing length scale is clearly evident as ρ increases. Pictures of space-time configurations containing correlated dynamical regions of size close to $\ell_{\max}$ at densities 0.77 in the (2)-TLG and 0.95 in the (1)-TLG are given in the lower left panels of Figs. 10 and 11, respectively. It is important to note that, in general, $\ell_{\max} \neq \ell^*$ [19]. Figure 12(c) shows the value of $\ell_{\max}$ plotted versus the structural relaxation time for both the (2)-TLG and the (1)-TLG. At short relaxation times, the curves merge and approach the ideal gas value of one. As relaxation times increases, the dynamical heterogeneity length scale for the strong version of the model is always larger than that of the fragile version at a fixed value of τ_α [15]. We also find that the observation time, $\Delta t_{\max}$, at which the maximum length scale, $\ell_{\max}$, occurs, scales with the structural relaxation time, τ_α, for both models (not shown).

If the (1)-TLG is in the universality class of the FA model, then we would expect $\ell_{\max}$ to scale as a power of both the excitation concentration, $\ell_{\max} \sim c^{-\nu}$, and of the relaxation time, $\ell_{\max} \sim \tau_\alpha^{1/z}$. This appears to be the case, as shown in Fig. 12(c). For the correlation and dynamic exponents we find $\nu \approx 0.89$ and $1/z \approx 0.36$, in reasonable agreement with Ref. [18], $\nu \approx 0.7$ and $1/z = \nu/\Delta \approx 0.3$ [36]. The z exponents shown in Fig. 12(c) are what we would expect from Fig. 12(b) where a range of $\ell(\Delta t)$ curves at different densities merge at early times and display power law scaling with similar exponents.

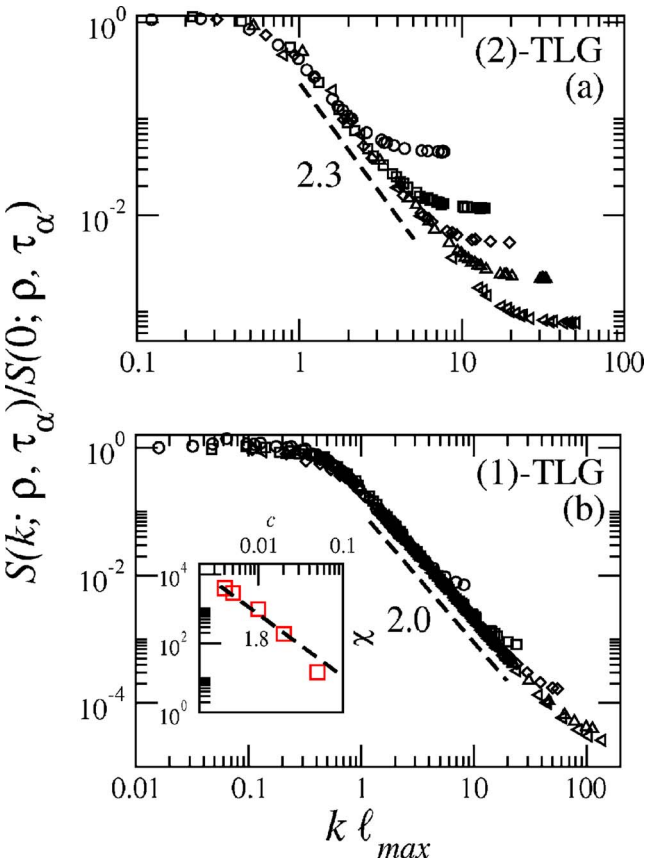

FIG. 13. (Color online) Structure factors of the mobility field, Eq. (3), measured at $\Delta t = \tau_\alpha$, for various densities in the (a) (2)-TLG and the (b) (1)-TLG. The axes are scaled as indicated.

As alluded to earlier, the dynamics of the (1)-TLG at high densities is controlled by the motion of vacancy pairs. The physics of these vacancy pairs is similar to excitations in the FA model. Vacancy pairs have the ability to interact with other lattice vacancies in order to branch and coalesce. It is important to note that evidence of these interactions can only be seen in simulations of large enough system sizes where the number of vacancy pairs is approximately 50–100. As mentioned in Sec. II, this requirement leads to system sizes, for example, of $L = 2048$ for $\rho = 0.995$.

Figure 13 shows the structure factors of the mobility field, Eq. (3), measured at the structural relaxation time, $\Delta t = \tau_\alpha$ for the (2)-TLG and the (1)-TLG. The curves are scaled in a manner suggestive of a coarsening process. The collapse of the various structure factors [37] implies that, in the glassy regime, increasing density corresponds to a coarsening of dynamic heterogeneity fields in space-time. An appreciation for the self-similarity of dynamic heterogeneity fields at different temperatures has already been noted in spin-facilitated models [15,18].

Both sets of scaled structure factors in Fig. 13 have an intermediate power law regime going as $k^{-2.3}$ for the (2)-TLG and k^{-2} for the (1)-TLG. One explanation for the difference in exponents could be the following. Porod law scaling, $k^{-(d+1)}$, arises from a system which is extensive in interfaces. In two dimensions, this implies that a system with a scaling exponent closer to 3 would have smoother interfaces. This interpretation is consistent with the snapshots of the dynamic heterogeneity fields in Figs. 10 and 11.

The structure factors for the (1)-TLG imply a value of the dynamical exponent η very close to zero, $S(k) \sim 1/k^{2-\eta}$ as $k \to \infty$. This gives a prediction for the exponent γ via the scaling relation $\gamma = (2-\eta)\nu_\perp$ of $\gamma \approx 1.8$. The γ exponent controls the scaling of the dynamic susceptibility, $\chi \equiv S(0;\rho,\tau_\alpha)$ with the concentration of excitations. The inset to Fig. 13(b) shows that this expectation is approximately satisfied [18].

VII. DISCUSSION

Despite their simplicity, the constrained lattice gas models we have studied show the essential features of glass forming liquids, such as a precipitous dynamical slowdown and dynamical heterogeneity. They are intermediate between the fully coarse grained kinetically constrained spin models such as the FA and East models, and atomistic models such as the binary Lennard-Jones mixture. We find a broad distribution of persistence times, especially in the (2)-TLG (Fig. 1). From the scaling of the structural relaxation time it follows that the (2)-TLG is a fragile model and the (1)-TLG is a strong one, consistent with the predicted scaling of the self-diffusion constant in [5,10]. Fragile behavior versus nonfragile behavior coincides with hierarchical versus diffusive propagation of excitations [5,38], and the former follows from directional persistence [15] as evident from the patterns of dynamic heterogeneity seen in Figs. 10 and 11. Dynamic heterogeneity produces length-time scaling and decoupling phenomena. Dynamic heterogeneity is present in both strong and fragile materials, not only in the latter. This is consistent with recent molecular dynamics simulation on silica [39] and earlier theoretical predictions [15,16].

ACKNOWLEDGMENTS

We are grateful to Robert Jack for important discussions. This work was supported by the U.S. National Science Foundation, by the U.S. Department of Energy Grant No. DE-FE-FG03-87ER13793, by EPSRC Grants No. GR/R83712/01 and GR/S54074/01, and University of Nottingham Grant No. FEF 3024. This research used resources of the National Energy Research Scientific Computing Center, which is supported by the Office of Science of the U.S. Department of Energy under Contract No. DE-AC03-76SF00098.

[1] M. D. Ediger, C. A. Angell, and S. R. Nagel, J. Phys. Chem. **100**, 13200 (1996).
[2] C. A. Angell, Science **267**, 1924 (1995).
[3] P. G. Debenedetti and F. H. Stillinger, Nature (London) **410**, 259 (2001).
[4] W. Kob and H. C. Andersen, Phys. Rev. E **48**, 4364 (1993).
[5] J. Jäckle and A. Krönig, J. Phys.: Condens. Matter **6**, 7633 (1994); A. Krönig and J. Jäckle, *ibid.* **6**, 7655 (1994).
[6] F. Ritort and P. Sollich, Adv. Phys. **52**, 219 (2003).
[7] D. Kivelson, S. A. Kivelson, X. L. Zhao, Z. Nussinov, and G. Tarjus, Physica A **219**, 27 (1995).
[8] X. Xia and P. G. Wolynes, Proc. Natl. Acad. Sci. U.S.A. **97**, 2990 (2000); J.-P. Bouchaud and G. Biroli, J. Chem. Phys. **121**, 7347 (2004).
[9] J. Kurchan, L. Peliti, and M. Sellito, Europhys. Lett. **39**, 365 (1997).
[10] C. Toninelli, G. Biroli, and D. S. Fisher, Phys. Rev. Lett. **92**, 185504 (2004); C. Toninelli and G. Biroli, J. Stat. Phys. **117**, 27 (2004).
[11] E. Marinari and E. Pitard, Europhys. Lett. **69**, 235 (2005).
[12] M. D. Ediger, Annu. Rev. Phys. Chem. **51**, 99 (2000).
[13] S. C. Glotzer, J. Non-Cryst. Solids **274**, 342 (2000).
[14] D. N. Perera and P. Harrowell, J. Chem. Phys. **111**, 5441 (1999).
[15] J. P. Garrahan and D. Chandler, Phys. Rev. Lett. **89**, 035704 (2002); Proc. Natl. Acad. Sci. U.S.A. **100**, 9710 (2003).
[16] L. Berthier and J. P. Garrahan, J. Chem. Phys. **119**, 4367 (2003); Phys. Rev. E **68**, 041201 (2003).
[17] Y. J. Jung, J. P. Garrahan, and D. Chandler, Phys. Rev. E **69**, 061205 (2004).
[18] S. Whitelam, L. Berthier, and J. P. Garrahan, Phys. Rev. Lett. **92**, 185705 (2004); Phys. Rev. E **71**, 026128 (2005).
[19] L. Berthier, D. Chandler, and J. P. Garrahan, Europhys. Lett. **69**, 320 (2005).
[20] A. C. Pan, J. P. Garrahan, and D. Chandler, Chem. Phys. Chem. **6**, 1783 (2005).
[21] The wave-vector dependent quantity, $F_s(q,t)$, was calculated as a Fourier transform on the square lattice. A correspondence can be made between the reciprocal lattice vectors of the square and triangular lattices as in [5].
[22] M. E. J. Newman and G. T. Barkema, *Monte Carlo Methods in Statistical Physics* (Oxford University Press, Oxford, 1999).
[23] R. Yamamoto and A. Onuki, Phys. Rev. E **58**, 3515 (1998).
[24] D. Richter, B. Frick, and B. Farago, Phys. Rev. Lett. **61**, 2465 (1988).
[25] W. Götze and L. Sjögren, Rep. Prog. Phys. **55**, 55 (1992).
[26] An alternative explanation is that relaxation in the (1)-TLG can simply be accounted for by the free diffusion of vacancy pairs, with interactions playing no role asymptotically. In that case τ_α would scale as c^{-2} and the deviations measured numerically would correspond to logarithmic corrections characteristic of two-dimensional diffusion. This is the situation, for example, in the square-plaquette spin model [27].
[27] R. Jack, L. Berthier, and J. P. Garrahan, Phys. Rev. E **72**, 016103 (2005).
[28] S. F. Swallen, P. A. Bonvallet, R. J. McMahon, and M. D.

Ediger, Phys. Rev. Lett. **90**, 015901 (2003).
[29] I. Chang and H. Sillescu, J. Phys. Chem. B **101**, 8794 (1997).
[30] K. S. Schweizer and E. J. Saltzman, J. Phys. Chem. B **108**, 19729 (2004).
[31] L. Berthier, Phys. Rev. E **69**, 020201(R) (2004).
[32] M. D. Ediger *et al.* (unpublished).
[33] L. Berthier and J. P. Garrahan, J. Phys. Chem. B **109**, 3578 (2005).
[34] N. Lacevic, F. W. Starr, T. B. Schrøder, and S. C. Glotzer, J. Chem. Phys. **119**, 7372 (2003).
[35] J. G. Amar, F. E. Sullivan, and R. D. Mountain, Phys. Rev. B **37**, 196 (1988).
[36] If interactions play no role in the (1)-TLG, then we would expect to observe $\nu=1$ and $z=2$.
[37] The discrepancy at large k is due to probing the granularity of the lattice.
[38] R. G. Palmer, D. L. Stein, E. Abrahams, and P. W. Anderson, Phys. Rev. Lett. **53**, 958 (1984).
[39] M. Vogel and S. C. Glotzer, Phys. Rev. Lett. **92**, 255901 (2004).